Faraday Discussions

Accepted Manuscript

This manuscript will be presented and discussed at a forthcoming Faraday Discussion meeting. All delegates can contribute to the discussion which will be included in the final volume.

Register now to attend! Full details of all upcoming meetings: http://rsc.li/fd-upcoming-meetings

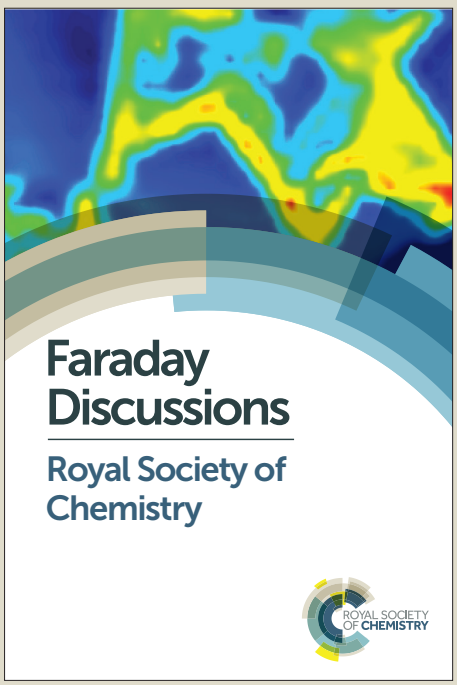

This is an *Accepted Manuscript*, which has been through the Royal Society of Chemistry peer review process and has been accepted for publication.

Accepted Manuscripts are published online shortly after acceptance, before technical editing, formatting and proof reading. Using this free service, authors can make their results available to the community, in citable form, before we publish the edited article. We will replace this *Accepted Manuscript* with the edited and formatted *Advance Article* as soon as it is available.

You can find more information about *Accepted Manuscripts* in the Information for Authors.

Please note that technical editing may introduce minor changes to the text and/or graphics, which may alter content. The journal's standard Terms & Conditions and the Ethical guidelines still apply. In no event shall the Royal Society of Chemistry be held responsible for any errors or omissions in this *Accepted Manuscript* or any consequences arising from the use of any information it contains.

ROYAL SOCIETY OF CHEMISTRY

www.rsc.org/faraday_d

Journal Name

ARTICLE TYPE

Cite this: DOI: 10.1039/xxxxxxxxxx

Photorelaxation of Imidazole and Adenine via Electron-Driven Proton Transfer Along H_2O Wires†

Rafał Szabla,*[a] Robert W. Góra,*[b] Mikołaj Janicki,[b] and Jiří Šponer[a,c]

Received Date
Accepted Date

DOI: 10.1039/xxxxxxxxxx

www.rsc.org/journalname

Photochemically created $\pi\sigma^*$ states were classified among the most prominent factors determining the ultrafast radiationless deactivation and photostability of many biomolecular building blocks. In the past two decades, the gas phase photochemistry of $\pi\sigma^*$ excitations was extensively investigated and was attributed to N–H and O–H bond fission processes. However, complete understanding of the complex photorelaxation pathways of $\pi\sigma^*$ states in aqueous environment was very challenging, owing to the direct participation of solvent molecules in the excited-state deactivation. Here, we present non-adiabatic molecular dynamics simulations and potential energy surface calculations of photoexcited imidazole-$(H_2O)_5$ cluster using the algebraic diagrammatic construction method to the second-order [ADC(2)]. We show that electron driven proton transfer (EDPT) along a wire of at least two water molecules may lead to the formation of a $\pi\sigma^*/S_0$ state crossing, similarly to what we suggested for 2-aminooxazole. We expand on our previous findings by direct comparison of the imidazole-$(H_2O)_5$ cluster to non-adiabatic molecular dynamics simulations of imidazole in the gas phase, which reveal that the presence of water molecules extends the overall excited-state lifetime of the chromophore. To embed the results in a biological context, we provide calculations of potential energy surface cuts for the analogous photorelaxation mechanism present in adenine, which contains an imidazole ring in its structure.

1 Introduction

Gas-phase photochemistry of small and medium-sized biomolecular building blocks has been intensively investigated during the past two decades.[1–3] These experimental and theoretical efforts enabled to identify multiple sub-picosecond radiationless photodeactivation mechanisms which elucidate the

[a] Institute of Biophysics, Academy of Sciences of the Czech Republic, Královopolská 135, 61265, Brno, Czech Republic; E-mail: rafal.szabla@gmail.com
[b] Department of Physical and Quantum Chemistry, Faculty of Chemistry, Wrocław University of Technology, Wybrzeże Wyspiańskiego 27, 50-370 Wrocław, Poland; E-mail: robert.gora@pwr.edu.pl
[c] CEITEC–Central European Institute of Technology, Masaryk University, Campus Bohunice, Kamenice 5, CZ-62500 Brno, Czech Republic

† Electronic Supplementary Information (ESI) available: [including geometrical parameters of selected structures and complete tables with vertical excitation energies]. See DOI: 10.1039/b000000x/

intrinsic photostability of isolated nucleobases, nucleosides and small peptides.[1,2,4,5] The most prominent of these photorelaxation channels are related to puckering of aromatic rings,[6] electron-driven proton transfer (EDPT)[5,7–9] and N–H (or O–H) bond fission processes,[10] which lead to conical intersections of the S_1 and S_0 states. Such ultrafast mechanisms preserve biomolecules from the deleterious effects of UV-irradiation, and thus it is often postulated that UV light played a major role at the early stages of chemical evolution on Archean Earth.[1,11]

Recent studies demonstrated that the photochemistry of organic molecules can be significantly altered by their interaction with the environment in the photoexcited state. In consequence, conclusions drawn based on experiments and simulations performed in the gas phase are not necessarily transferable to more biologically or chemically relevant systems in bulk. For instance, 2-aminopurine is characterized by sub-picosecond excited-state lifetime in the gas phase, whereas microhydration of the molecule results in time constants up to ∼100 times larger,[12] owing to exchanged ordering of the $\pi\pi^*$ and $n\pi^*$ states.[13] On the other hand, the presence of sugar moiety in nucleosides may result in excited-state proton transfer or hydrogen atom abstraction processes, not present in isolated nucleobases.[14–16] In the case of oligonucleotides, base stacking enables the formation of charge-transfer electronic states within two adjacent purine bases,[17–19] which also exhibit extended excited-state lifetimes or might even participate in the self-repair of cyclobutane pyrimidine dimer DNA photolesions.[20] Finally, it was shown that strongly interacting solvents may participate in the formation of state crossings, and thus, open new photorelaxation channels not available in the gas phase, in molecules like adenine,[21–23] 4-aminoimidazole-5-carbonitrile (AICN)[24] or 2-aminooxazole (AMOX).[25]

Repulsive $\pi\sigma^*$ states exhibit a particularly interesting photochemistry which can be directly modified by surrounding solvent molecules. The N–H and O–H bond fission processes leading to $\pi\sigma^*/S_0$ conical intersections in isolated organic chromophores,[10,26–28] are either not observed or unimportant in the aqueous environment.[25,29] Instead, microhydrated chromophores which exhibit characteristic $\pi\sigma^*$ photochemistry release an electron towards the surrounding water molecules, which is often referred to as the charge transfer to solvent (CTTS).[29–32] Thus created hydrated electron may be further followed by a proton transfered from the chromophore towards the nearest water molecule yielding a H_3O^+ cation and a hydrated electron delocalized on the remaining water molecules in the cluster.[29] The formation of e^-_{aq}, H_3O^+ and phenoxyl radicals upon the photoexcitation of phenol in bulk water was also confirmed by transient absorption spectroscopy measurements.[33] Recently, we demonstrated

that one or more subsequent proton transfers from the H_3O^+ cation in the direction of the hydrated electron lead to the formation of a $\pi\sigma^*/S_0$ state crossing.[24,25] This mechanism was reported for AICN and AMOX, based on potential-energy (PE) surface explorations and nonadiabatic molecular dynamics simulations. Independently, Atealahi *et al.*[34] reported on an analogous deactivation mechanism which operates in hydroquinone and catechol clustered with ammonia. These findings challenge the previous suggestions that microsolvation removes $\pi\sigma^*/S_0$ conical intersections,[29,35] and imply that $\pi\sigma^*$-mediated photorelaxation mechanisms are only modified and might be relevant also in bulk environments. In our previous study of microsolvated AMOX, we called this photorelaxation mechanism electron-driven proton transfer (EDPT) along H_2O wires,[25] due to the decoupled movement of the electron and proton.[36] It is worth noting, that some authors use the term sequential proton-coupled electron transfer (PCET) to describe analogous processes.[37]

The influence of water on the excited-state dynamics of adenine was recently studied by means of ultrafast pump-probe spectroscopic approaches and electronic structure calculations.[21–23,38–44] Nonadiabatic molecular dynamics simulations of microhydrated 7H-adenine (which constitutes ∼20% of adenine dissolved in water at standard ambient conditions), revealed yet another previously unknown photorelaxation mechanism based on water-to-chromophore electron transfer.[21] EDPT from water to the N3 atom of adenine was also reported as a plausible photodeactivation pathway of 9H-adenine, based on the excited-state dynamics simulations and PE surface computations.[22,23] Nonetheless, none of the previous theoretical studies addressed the $\pi\sigma^*$ mediated EDPT mechanism in aqueous adenine, while the distinctive N–H bond fission mechanism was reported for adenine in the gas phase.[45–49] Experimental investigations of hydrated adenine yielded somewhat contradictory conclusions regarding the importance of $\pi\sigma^*_{NH}$ states. In particular, Ritze *et al.*[40] proposed that microhydration of adenine significantly stabilizes $\pi\sigma^*_{NH}$ states and facilitates the corresponding deactivation mechanisms. Similarly, Pancur and co-workers[38] suggested that the decrease of the excited-state lifetime of 9H-adenine at excitation wavelengths $\leq$265 nm might be ascribed to the involvement of $\pi\sigma^*$ states in the photorelaxation of this molecule in aqueous solution. In contrast, ultrafast transient electronic and vibrational absorption spectroscopic studies of adenine in bulk water suggest that $\pi\sigma^*$ states are not involved in the photodeactivation of the molecule for $\lambda_{exc} \geq$220 nm.[42]

Here, we try to address this problem by means of PE surface computations and analysis of the corresponding minimum-energy crossing points (MECPs) of microhydrated adenine. We also discuss

the results of nonadiabatic molecular dynamics simulations of a relevant model chromophore, namely imidazole and its cluster with 5 water molecules. Since adenine constitutes an imidazole ring in its structure, this allows us to thoroughly characterize the $\pi\sigma^*$-mediated EDPT along H_2O wires photorelaxation pathway found in both microsolvated molecules.

2 Computational Methods

The ground-state minimum-energy geometries and harmonic vibrational frequencies of imidazole, adenine and their clusters with 5 water molecules were estimated using the Kohn–Sham density functional theory (KS-DFT) with the def2-TZVP basis set[50] and the B3LYP hybrid functional.[51] The geometries of such obtained hydrogen-bonded complexes should be close to the MP2 optimized reference structures.[52] Although the corresponding relative stabilities of various isomers might not be equally well reproduced,[53] in this study we are not attempting nor relying on such predictions. Subsequent computations of vertical excitation energies, simulations of UV-vis spectra, optimizations of the minimum-energy structures on the $\pi\sigma^*$ hypersurface, and nonadiabatic molecular dynamics simulations were performed employing the algebraic diagrammatic construction method to the second-order [ADC(2)][54–56] and the correlation-consistent aug-cc-pVDZ basis set.[57,58] The PE surface scans in chromophore-water clusters were performed by means of linear interpolations in internal coordinates (LIIC) between the appropriate stationary points on the excited state PE surface. The PE surface scans along the N–H bonds of isolated imidazole and adenine were constructed by elongation of the N–H bond stretching coordinate and keeping all the remaining coordinates fixed at the ground state geometry. Thus obtained rigid PE surface scans provide a sufficiently reliable description of the photoinduced N–H bond fission, since it is an ultrafast photoreaction and the remaining nuclear coordinates do not vary significantly within the ultrashort timescale of this process. The corresponding energies of the excited states were obtained at the ADC(2)/aug-cc-pVDZ level of theory, whereas the MP2/aug-cc-pVDZ approach was used for the calculation of the ground-state energies. The S_1/S_0 minimum-energy crossing points (MECPs) were optimized at the ADC(2)/MP2 level using the CIOpt program of Levine, Martinez and Coe,[59] which allows to optimize MECPs without evaluating the nonadiabatic couplings. This optimization protocol was recently tested for retinal chromophore model and proved to provide a reliable geometry of the $\pi\pi^*/S_0$ conical intersection in this molecule.[60]

The UV-vis absorption spectra were simulated using the nuclear ensemble method.[61] In this pro-

cedure, 500 points were obtained from a Wigner distribution for all vibrational normal modes of the ground-state geometries of the isolated imidazole molecule and imidazole-$(H_2O)_5$ cluster. The initial conditions for the nonadiabatic molecular dynamics simulations were sampled from the 6.17±0.06 spectral window (around 200.8 nm, see Fig. 2) in both systems, similarly as in the previous joint experimental and theoretical study of imidazole in the gas phase.[62] Six lowest-lying excited electronic states were considered in the spectra simulations and in the following excited state dynamics simulations. The semi-classical nonadiabatic molecular dynamics simulations were performed employing the Tully's fewest-switches surface hopping algorithm with decoherence correction of Granucci and Persico (with the decoherence parameter of 0.1 Hartree).[63] The time step of 0.025 fs was applied to the semi-classical approximation of the electronic time-dependent Schrödinger equation, while the time step for propagation of the classical equations for nuclear motion was set to 0.5 fs. 69 and 54 trajectories were simulated for the isolated imidazole and imidazole–$(H_2O)_5$ cluster for up to 600 fs, or until the energy gap between the S_1 and S_0 states dropped below 0.15 eV. The latter is due to a fact that the ADC(2) method becomes unreliable in the vicinity of conical intersections with the ground state. Therefore, the nonadiabatic transitions were enabled only between the excited electronic states. This approach enabled to identify the photodeactivation channels and to estimate the excited-state lifetimes of the studied molecules. Such a computational scheme was already applied and carefully tested against experimentally obtained photorelaxation time constants and nonadiabatic molecular dynamics simulations performed at the MRCIS level.[21,45]

All the KS-DFT, ADC(2) and MP2 electronic structure calculations were performed with the Turbomole 7.0.2 program.[64] The UV-vis spectra and nonadiabatic molecular dynamics simulations were conducted using the Newton-X 1.4 package.[65]

3 Results and Discussion

Equilibrium geometries of the S_0 and $\pi\sigma^*_{NH}$ states

As reported for AICN and AMOX, the number and position of water molecules clustered with the chromophore influences the properties of the $\pi\sigma^*_{NH}$ state.[24,25] In particular, we observed that at least 5 water molecules are necessary to stabilize the H_3O^+ cation and hydrated electron during the excited-state dynamics on the $\pi\sigma^*$ hypersurface.[24,25] Therefore, we placed clusters of 5 water molecules on the side of the N–H bonds which were found to dissociate upon the photoexcitation of imidazole

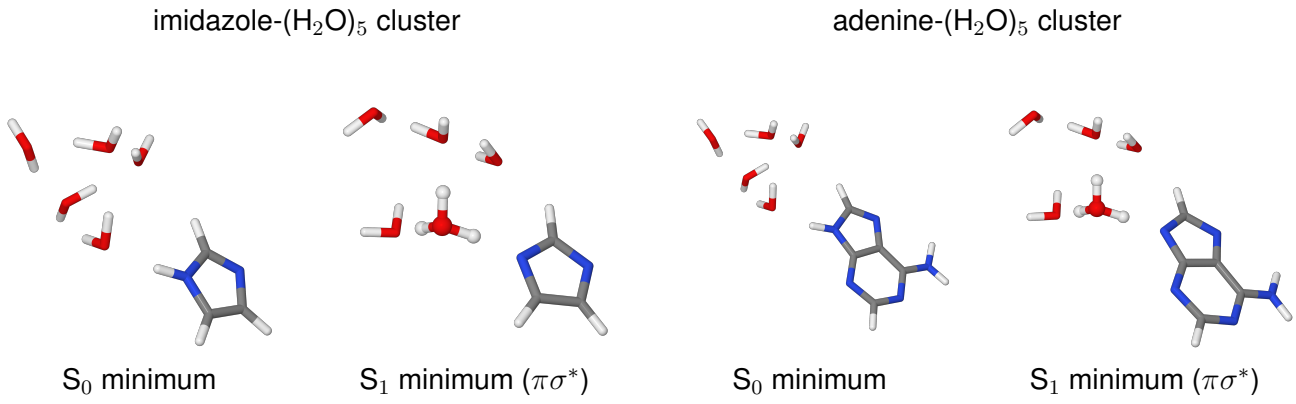

Fig. 1 Optimized geometries of the ground and $\pi\sigma^*$ (S_1) electronic states of imidazole and adenine clustered with 5 water molecules.

and adenine in the gas phase. The respective ground-state equilibrium geometries of the imidazole-$(H_2O)_5$ and adenine-$(H_2O)_5$ clusters are presented in Fig. 1. It should be noted that the structures of these complexes are not necessarily the most stable ones but rather the most suitable to facilitate the formation of conical intersection via the subsequent proton transfers occurring on the $\pi\sigma^*$ hypersurface. In our previous studies we observed that at least two such transfers are required after formation of the hydrated electron, in which the H_3O^+ cation is formed.[24,25] We also analyzed systematically extended clusters with up to 7 water molecules and established that such a topology of the model cluster is optimal considering the computational accuracy and feasibility. However, it is interesting to note that the selected model complex is very similar to the lowest-energy structure of AMOX-$(H_2O)_5$, determined by Calvo *et al.*[66] In each of the cases we located also the minimum energy structure of the $\pi\sigma^*_{NH}$ state, which consists of an imidazole (or adenine) radical, H_3O^+ cation and the hydrated electron shielded from the remaining part of the cluster by 4 water molecules.

Vertical excitation energies and UV-vis spectra of isolated molecules and their clusters

The vertical excitation energies of the relevant electronic states involved in the photochemistry of isolated imidazole and adenine, and their water clusters are presented in Tab. 1. Complete tables containing all 5 lowest-lying electronic excitations for each system can be found in the Supporting Information to this article. Our results for the gas-phase molecules are generally consistent with the previously reported data[45,62,67,68] and here we wish to discuss only the states that are relevant for the present study.

Table 1 Selected vertical excitation energies (in eV) of imidazole and adenine in the gas phase and their corresponding clusters with 5 water molecules, computed using the ADC(2)/aug-cc-pVDZ method assuming the ground-state minimum energy structures optimized at the B3LYP/def2-TZVP level.

State / Transition		E_{exc}/[eV]	f_{osc}	λ/[nm]
imidazole (gas phase)				
S_1	$\pi\sigma^*_{NH}$	5.56	$7.77 \cdot 10^{-4}$	223.0
S_4	$\pi\pi^*$	6.52	0.167	190.2
imidazole–$(H_2O)_5$ cluster				
S_1	$\pi\sigma^*_{NH}$	5.50	$3.55 \cdot 10^{-3}$	225.4
S_3	$\pi\pi^*(\pi-3p)$	6.10	$8.64 \cdot 10^{-2}$	203.4
adenine (gas phase)				
S_1	$n\pi^*$	5.09	$2.67 \cdot 10^{-3}$	243.7
S_2	$\pi\pi^*$	5.19	0.239	238.9
S_4	$\pi\sigma^*_{NH}$	5.36	$1.03 \cdot 10^{-2}$	231.5
adenine–$(H_2O)_5$ cluster				
S_1	$n\pi^*$	5.07	$7.95 \cdot 10^{-3}$	244.4
S_3	$\pi\pi^*$	5.22	0.192	237.5
S_5	$\pi\sigma^*_{NH}$	5.49	$1.48 \cdot 10^{-3}$	226.0

The lowest-lying excited singlet state of both isolated imidazole and imidazole-$(H_2O)_5$ cluster is the $\pi\sigma^*_{NH}$ state, having considerable Rydberg character and being repulsive with respect to the N–H bond stretch. Since the $\pi\sigma^*_{NH}$ excitation is significantly separated from the remaining excited electronic states, it becomes evident that N–H bond fission should be the dominant photorelaxation pathway of imidazole and its cluster. In spite of the considerable electric dipole moment of this state (6.99 D), its excitation energy is scarcely affected by the microhydration. In contrast, the optically bright $\pi\pi^*$ excitation of imidazole is considerably red-shifted in the cluster by $\sim$0.4 eV. This feature is also visible in the simulated UV-vis spectra (cf. Fig. 2) in which the absorption maximum of the imidazole-$(H_2O)_5$ cluster is red-shifted by 0.4-0.5 eV with respect to the spectrum of isolated imidazole. This is due to change in the character of this state upon microsolvation. Although in the gas phase this transition shows already some valence-Rydberg mixing, in the cluster it gains strong charge transfer to solvent $\pi - 3p$ component.

The two lowest-lying excited singlet states of adenine are of $n\pi^*$ and $\pi\pi^*$ character, and these states dominate the photodynamics of this molecule as described before.[45] The estimated excitation

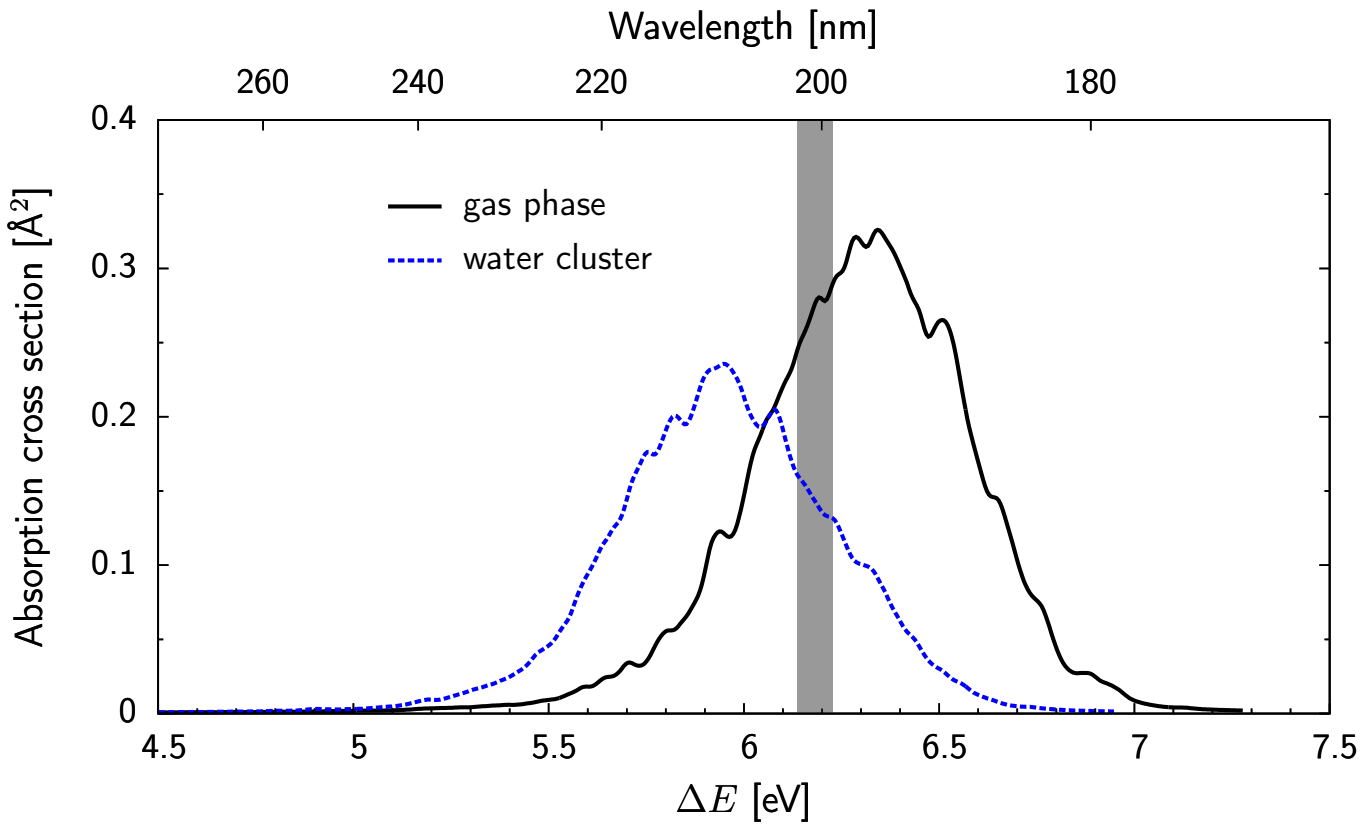

Fig. 2 UV absorption spectrum of imidazole in the gas phase and imidazole-$(H_2O)_5$ cluster simulated at the ADC(2)/aug-cc-pVDZ level. The initial conditions were sampled from the shaded area of the spectrum (6.17±0.06 eV).

energy of the $\pi\sigma^*_{NH}$ state in the gas phase amounts to 5.36 eV (231.5 nm) and is in good agreement with the H atom photofragment translational energy spectra of Nix *et al.*,[48] who reported on the onset for $\pi\sigma^*$ mediated N–H bond rupture for excitation wavelengths $\leq$233 nm. In contrast to the imidazole-$(H_2O)_5$ cluster, the excitation energy of the $\pi\sigma^*_{NH}$ state of the adenine-$(H_2O)_5$ cluster is slightly blue-shifted (by $\sim$0.15 eV), which indicates that the $\pi\sigma^*$ mediated EDPT photorelaxation channel might be even less accessible in aqueous environment. The optically bright $\pi\pi^*$ state of adenine is virtually unaffected by the neighbouring water molecules. Even though our model cluster does not reproduce all the solvation effects exerted by bulk water, the calculations of Yamazaki and Kato,[44] which aimed to reproduce bulk solvation effects, suggest similar trends. In particular, the authors also observed a hypsochromic shift of the repulsive $\pi\sigma^*_{NH}$ state.

Nonadiabatic molecular dynamics simulations

Our photodynamics simulations reveal interesting differences between imidazole in the gas phase and its water cluster. This can be inferred, for instance, from the time evolution of the occupations of each adiabatic state presented in Fig. 3, where only four excited states are shown for clarity. In the case of isolated imidazole, the fractional occupations of the S_2 and higher excited states drop rapidly after the first 10 fs of the simulation and approach nearly 0 after 100 fs. At the same time the occupation of the S_1 state rises until ~50 fs and starts to decline efficiently afterwards until the ground electronic state is fully populated at 408 fs. In the case of imidazole-$(H_2O)_5$ cluster, we see much slower depopulation of the higher excited states, which persist on a discernible level for approximately 200 fs. Interestingly, the occupation of the S_2 state rises significantly during the initial 20 fs of the photodynamics, and after 100 fs its depopulation correlates with that of the S_1 state. Maximum occupation of the S_1 state is reached at ~80 fs and then slowly declines until the maximum simulation time of 600 fs is reached. A small fraction of trajectories (0.037) simulated for the imidazole-$(H_2O)_5$ cluster, did not undergo photorelaxation to the ground state within this time period. It is worth noting, though, that the adiabatic state occupations shown in Fig. 3 do not account for the S_0 to S_1 "back-hoppings" due to limitations of the ADC(2) method discussed in the computational section. Therefore, trajectories for which the S_1-S_0 energy gap dropped below 0.15 eV were assumed to have reached the ground state, and terminated. Nonetheless, the above observations are sufficient to conclude that the radiationless deactivation of the cluster is much more complex when compared to that of isolated imidazole. Furthermore, the corresponding excited-state lifetime of microsolvated imidazole is visibly longer.

As proposed in the joint experimental and theoretical work by Crespo-Otero *et al.*,[62] the electronic ground state population of isolated imidazole can be fitted with the single exponential decay function:

$$f(t) = 1 - \exp\left[-\left(\frac{t}{\tau}\right)\right]. \quad (1)$$

Thus estimated time constant of 94 fs based on our ADC(2) simulations is in good agreement with the experimental value of 74±30 fs obtained from the equivalent excitation window.[62] Analogous nonadiabatic molecular dynamics simulations performed at the TDDFT level yielded a somewhat larger time constant of 117 fs.[62] The corresponding time constant estimated for the imidazole-$(H_2O)_5$ cluster

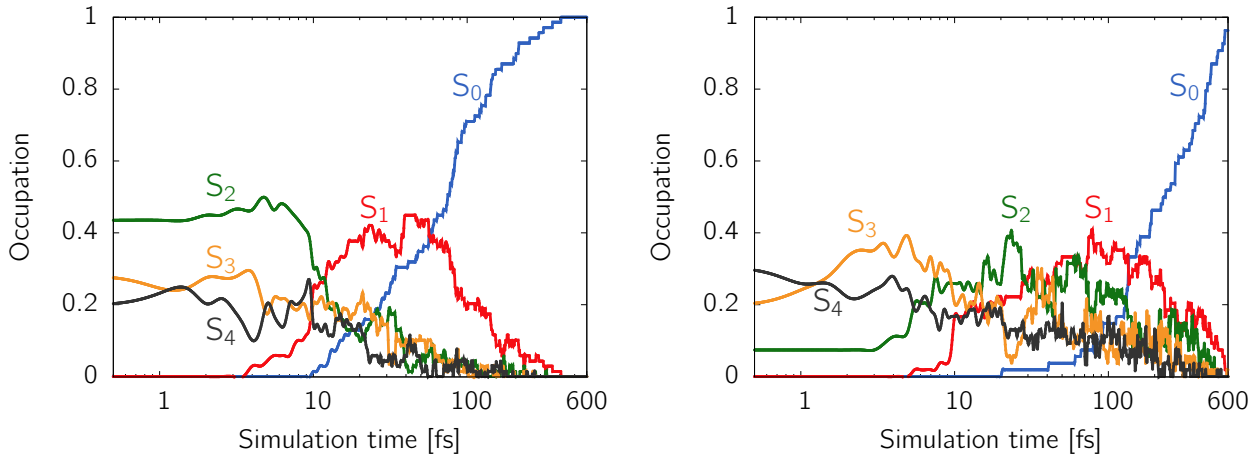

Fig. 3 Time evolution of the ground and excited states populations of imidazole molecule (left) and its water cluster (right).

amounts to 311 fs. Nevertheless, the obtained value should be treated rather tentatively owing to the limited number of trajectories simulated for the cluster, and the maximum simulation time of merely 0.6 ps. In fact, time evolution of the adiabatic state occupations, shown in Fig. 3, and the results of our previous simulations of the EDPT process in microsolvated AMOX molecule, indicate a more complex deactivation pattern, albeit reliable fitting of a multi-exponential function would require more data and longer simulation time.[25]

The radiationless deactivation of imidazole occurs either on the $\pi\pi^*$ hypersurface leading to puckering of the aromatic ring or follows the $\pi\sigma^*_{NH}$ mediated N–H bond fission mechanism. The latter photoreaction pathway was found to be dominant and corresponding to 83% of all photorelaxation events in isolated imidazole photoexcited within the equivalent spectral range (6.0-6.2 eV) and simulated using the TD-B3LYP approach.[62] Our simulations performed at the ADC(2) level indicate significantly lower contribution of the N–H bond fission processes (49.3%; see Fig. 4). However, the latter still remains the primary photorelaxation channel of imidazole in the gas phase. Apart from this, the ring-puckering mechanism was responsible for the photorelaxation of 42.0% of the trajectories, while the remaining 8.7% of trajectories reached the ring-opened conical intersection related to the rupture of the C–N bond. In the case of the imidazole-$(H_2O)_5$ cluster, 61.1% of the simulated trajectories accessed the $\pi\sigma^*/S_0$ state crossing via the EDPT photorelaxation pathway. This indicates even larger contribution of the $\pi\sigma^*_{NH}$ state to the photochemistry of microsolvated imidazole than in the isolated molecule. Puckering of the aromatic ring occurred twice less frequently than the EDPT mechanism.

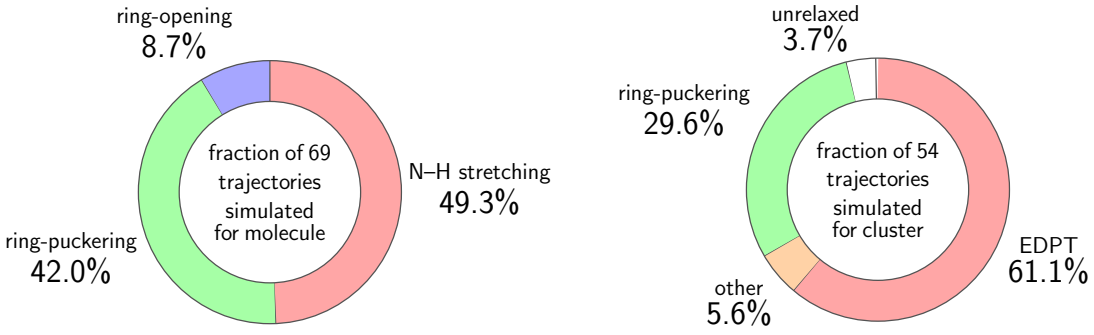

Fig. 4 Quantum yields of the photodeactivation processes calculated for the studied imidazole molecule (left) and imidazole-$(H_2O)_5$ cluster (right).

The remaining trajectories either followed other deactivation channels (mainly C–H bond fission) or did not reach the electronic ground state within 0.6 ps (3.7% of the trajectories). Interestingly, none of the trajectories simulated for the cluster followed the ring opening photorelaxation channel, which might be of paramount importance for the photostability of this and similar species in aqueous solution.

The N–H bond fission process which operates in the gas phase is significantly modified in the imidazole-$(H_2O)_5$ cluster due to the direct participation of water molecules in the formation of the state crossing. Similarly, as observed by Sobolewski and Domcke for microsolvated phenol, pyrrole and indole,[29–32] the electron excited to the diffuse σ^* orbital is solvated by the neighbouring water molecules and partly shielded from the chromophore. This $\pi\sigma^*$ mediated charge transfer to solvent event may be further followed by the N–H proton transfer to the nearest water molecule which results in the formation of an imidazole radical, H_3O^+ cation and hydrated electron.[29] Similarly as reported for AICN and AMOX clustered with water molecules,[24,25] at least one further proton transfer from the hydronium cation towards a water molecule directly interacting with e^-_{aq} is necessary to reach the $\pi\sigma^*/S_0$ intersection seam. This EDPT mechanism requires the mobile proton to move in the direction of the hydrated electron along a wire of two to three water molecules for the system to reach the electronic ground state. This implies that the decisive factor in the photodeactivation mechanism is the final relative position of the H_3O^+ cation with respect to the imidazole radical, instead of the number of proton transfers, which is mainly dependent on transient arrangement of the water cluster. 7 out of 32 trajectories, which followed the EDPT photorelaxation pathway reached a somewhat distinct $\pi\sigma^*/S_0$ conical intersection, accessed by the O–H bond dissociation of the initially formed H_3O^+ cation. However, this latter mechanism is rather unlikely to occur in bulk solutions and was

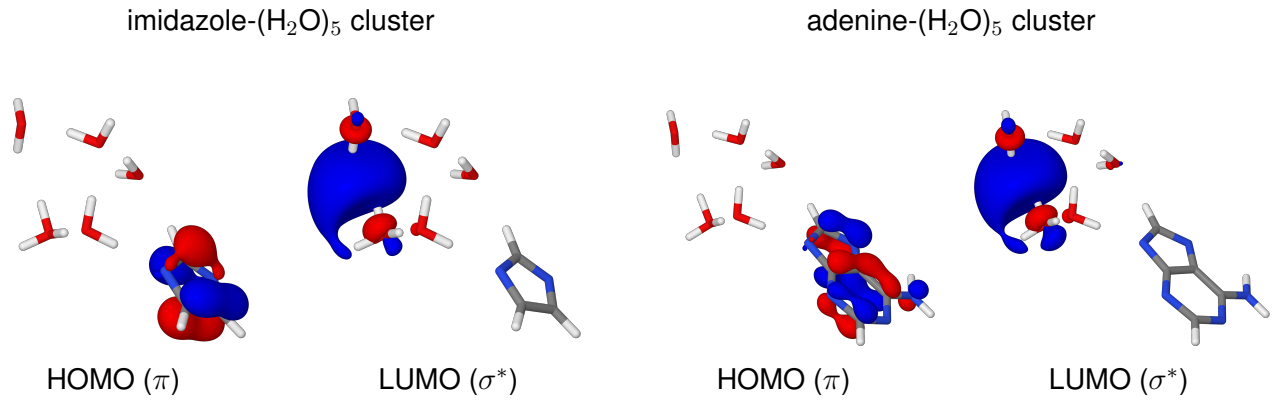

Fig. 5 S_1/S_0 MECP geometries corresponding to the EDPT photorelaxation channel of imidazole-$(H_2O)_5$ and adenine-$(H_2O)_5$ clusters, obtained using the ADC(2) and MP2 method for the S_1 and S_0 states,respectively, and the aug-cc-pVDZ basis set. The relevant π and σ^* molecular orbitals are shown for both clusters.

not observed in the nonadiabatic molecular dynamics simulations of AMOX-$(H_2O)_5$ cluster. In other words, it might be pertinent to small clusters only, since in bulk solution the dissociating proton can be readily intercepted by another water molecule from the surroundings.

While the photoinduced N–H bond rupture reported for molecules in the gas phase is a very rapid process, occurring on a sub-100 fs timescale,[10,26,62] EDPT along H_2O wires is associated with noticeably longer relaxation times. This is the consequence of the proton migrating towards the hydrated electron in two to three subsequent stages. In fact, the initial deprotonation of the N–H bond may be followed by multiple backward-forward proton transfers on the $\pi\sigma^*$ hypersurface, which periodically restore (and then again deprotonate) the initial form of imidazole. Only when the proton migrates closer towards the hydrated electron, the system may photorelax to the ground electronic state. If during the backward-forward proton transfers the system changes the character of the state (for instance to $\pi\pi^*$), the cluster may access any other type of S_1/S_0 conical intersection mentioned above. Therefore, the EDPT process may extend the timescale of any other radiationless deactivation pathway available in the cluster.

The most representative $\pi\sigma^*/S_0$ conical intersection geometry that can be accessed via the EDPT mechanism is shown in Fig. 5. This structure was optimized using the ADC(2)/MP2 methods and the procedure of Levine and co-workers (see the computational section for details). At the conical intersection the solvated electron which occupies the σ^* orbital is surrounded by three H_2O molecules and one H_3O^+ cation formed in the two-stage proton transfer from the imidazole molecule. To confirm

the plausibility of the EDPT mechanism in microsolvated adenine, we located an analogous conical intersection for this molecule which is structurally very similar to the state-crossing geometry located for imidazole (right-hand side of Fig. 5). The geometries shown in Fig. 5 are also characterized by slight elongation of the O–H bond pointing in the direction of the hydrated electron (up to ∼1.1 Å and ∼1.16 Å for the imidazole and adenine clusters), which is essential to reach the degeneracy of the S_1 and S_0 states.

Potential energy profiles for the EDPT along H_2O wires mechanism

The reaction-path potential energy profiles shown in Fig. 6 reveal further details of the EDPT mechanism responsible for the photorelaxation of microhydrated imidazole. The PE surfaces related to the $\pi\sigma^*$ mediated N–H bond fission mechanism operating in isolated imidazole are shown on the left-hand side of Fig. 6. This mechanism was described in detail previously, and we present it for direct comparison to the EDPT channel shown on the right-hand side of Fig. 6. In both cases the $\pi\sigma^*/S_0$ conical intersection can be accessed in a nearly barrierless manner. In the case of microsolvated imidazole, the insignificant barrier associated with the first proton transfer might, in fact, be an artifact of the LIIC procedure used to obtain intermediate geometries between the Franck–Condon region and the minimum of the $\pi\sigma^*$ state. This is confirmed by the fact that we did not locate a minimum on the $\pi\sigma^*$ surface which would precede N–H deprotonation and formation of the hydronium cation. Instead, during the initial stages of excited-state dynamics the imidazole-$(H_2O)_5$ cluster explores a plateau region on the $\pi\sigma^*$ hypersurface before descending to the S_1 minimum (also shown in Fig. 1) along the N–H proton transfer coordinate. In the minimum of the $\pi\sigma^*$ state the S_1-S_0 energy gap amounts to 1.70 eV and the N–H bond distance is equal to 1.63 Å. The second proton transfer leads eventually to the $\pi\sigma^*/S_0$ conical intersection when the O–H distance of 1.51 Å is reached. This minimum-energy crossing point optimized using the ADC(2)/MP2 methods lies 0.2 eV above the minimum on the $\pi\sigma^*$ surface. The EDPT photorelaxation channel is easily accessible in microsolvated imidazole since the corresponding $\pi\sigma^*$ state is the lowest-lying excited singlet for most nuclear configurations of the imidazole-$(H_2O)_5$ assembly.

The analogous PE profile showing the details of EDPT photorelaxation channel in adenine is shown in Fig. 7. This process, driven by the $\pi\sigma^*$ state of adenine, has most of the qualitative features described above for the imidazole-$(H_2O)_5$ cluster. Thus, there is only one minimum on the $\pi\sigma^*$ hyper-

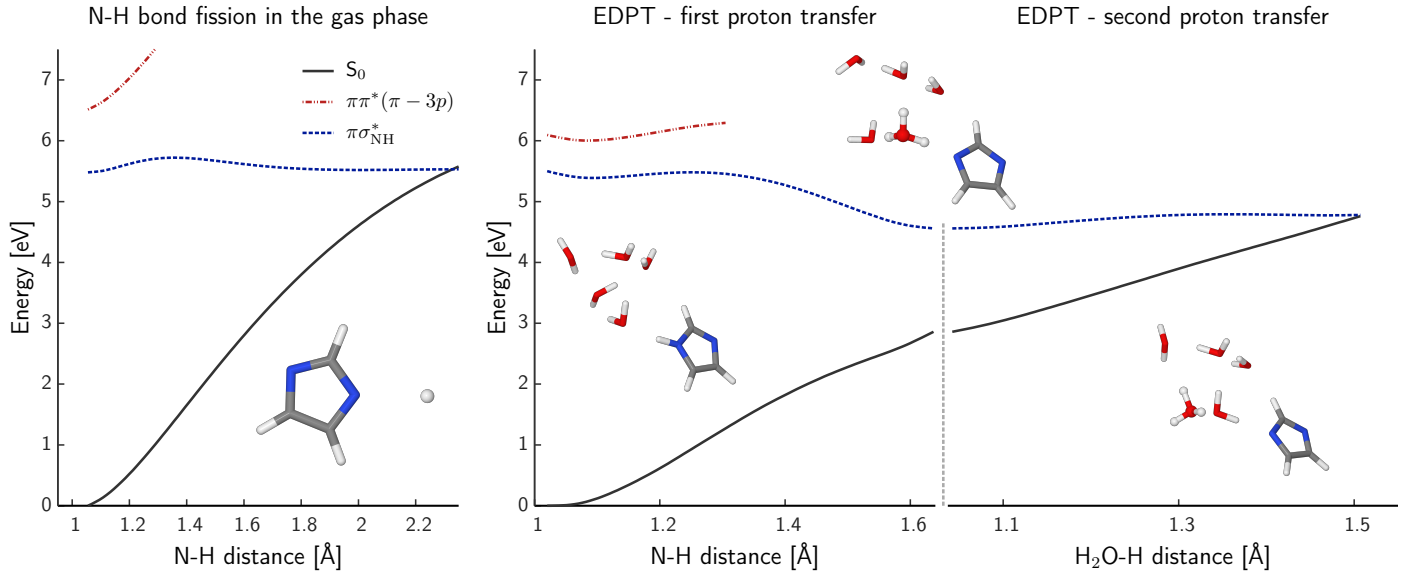

Fig. 6 Potential energy profiles presenting $\pi\sigma^*$-mediated photorelaxation pathways of imidazole and its water cluster. The PE profile for bare imidazole represents a rigid scan along the N–H distance initiated in the Franck-Condon region. The PE profiles for the imidazole-$(H_2O)_5$ cluster were constructed based on interpolations between the Franck–Condon region, minimum on the $\pi\sigma^*$ surface, and $\pi\sigma^*/S_0$ MECP. Excited-state energies were computed at the ADC(2)/aug-cc-pVDZ level.

surface (shown also in Fig. 1) of virtually identical character as in the case of the imidazole cluster. The S_1-S_0 energy gap calculated in the minimum of the $\pi\sigma^*$ state is slightly larger and amounts to nearly 2.0 eV. Our calculations indicate also slightly more sloped topography of the $\pi\sigma^*/S_0$ conical intersection, which lies 0.3 eV above the corresponding S_1 minimum. Perhaps the most prominent difference is the accessibility of the EDPT photorelaxation pathway, which will be significantly hindered in microsolvated adenine due to the low-lying $\pi\pi^*$ and $n\pi^*$ excitations in the UV-vis spectrum of adenine, and the solvent-induced blue-shift of the $\pi\sigma^*$ state (see Tab. 1 and the respective commentary in the text). Therefore, the onset of EDPT photorelaxation channel in aqueous adenine might be observed for excitation wavelengths even shorter than the threshold reported by Nix *et al.* for the N–H bond fission process of adenine in the gas phase.

4 Conclusions

In conclusion, we performed semi-classical nonadiabatic molecular dynamics simulations of imidazole in the gas phase and in a cluster containing 5 water molecules, using the ADC(2)/aug-cc-pVDZ approach for the electronic structure calculations. These results allowed us to directly compare the two $\pi\sigma^*$ driven photorelaxation processes in isolated and microhydrated chromophore, namely N–H bond fission and EDPT along H_2O wires. Therefore, we confirm our previous hypothesis that the pho-

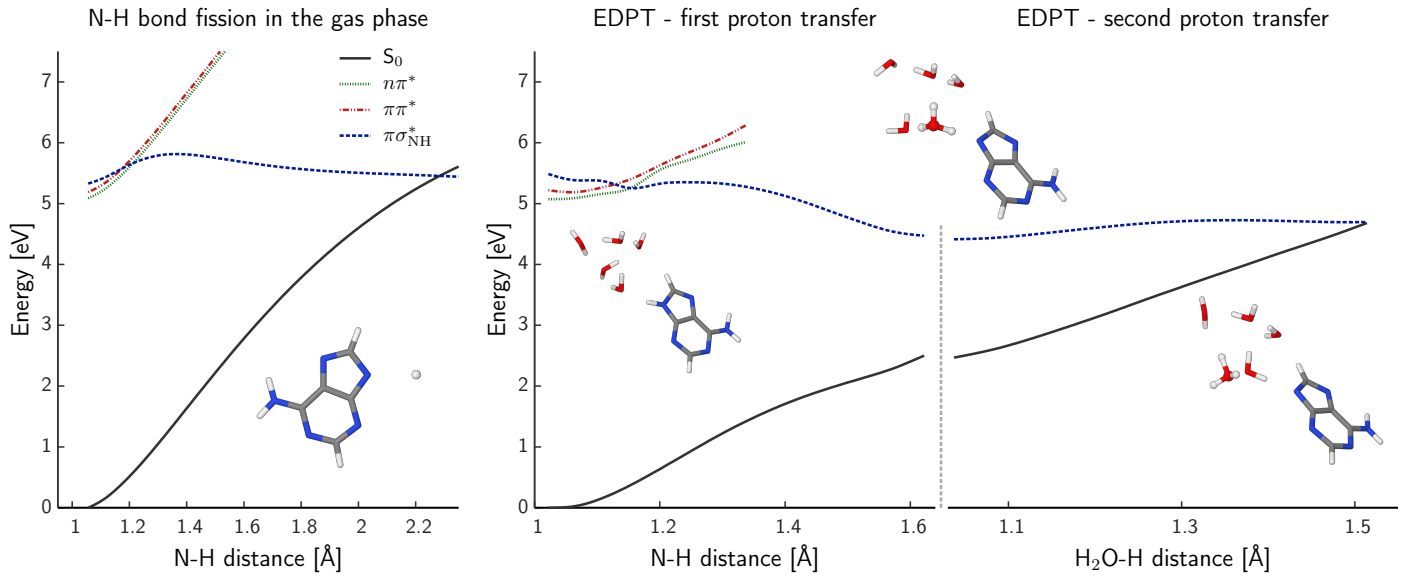

Fig. 7 Potential energy profiles presenting $\pi\sigma^*$ mediated photorelaxation pathways of bare and microsolvated adenine. The PE profile for gas-phase adenine represents a rigid scan along the N–H distance initiated in the Franck-Condon region. The PE profiles for the adenine-$(H_2O)_5$ cluster were constructed based on interpolations between the Franck–Condon region, minimum on the $\pi\sigma^*$ surface, and $\pi\sigma^*/S_0$ MECP. Excited-state energies were computed at the ADC(2)/aug-cc-pVDZ level.

torelaxation occurring on $\pi\sigma^*$ hypersurface is characterized by a much longer timescale in aqueous environment than in the gas phase. In particular, we show that the EDPT along H_2O wires process might play a dominant role in the photorelaxation of microsolvated imidazole. Even though the quantum yields of different photodeactivation processes might be affected by the internal arrangement of water molecules in the cluster, the separation of the $\pi\sigma^*$ state from other electronic excitations is large enough to assume the general importance of the EDPT mechanism for aquated imidazole. As stated previously, we suggest that this mechanism should be also relevant in bulk water.[24,25]

Calculations of the vertical excitation energies and PE profiles for isolated adenine and an analogous adenine-$(H_2O)_5$ cluster provide additional details about the plausibility of the $\pi\sigma^*$ mediated EDPT photorelaxation channel in this molecule. Since adenine contains an imidazole ring in its structure, it is quite intuitive that EDPT along H_2O wires might be one of the photorelaxation channels of aqueous adenine. However, the observed blue-shift of the $\pi\sigma^*$ state in the spectrum of the considered adenine-$(H_2O)_5$ cluster suggests much lower accessibility of this channel in comparison to the imidazole cluster. This argument is strengthened due to rather low excitation energies of the $\pi\pi^*$ and $n\pi^*$ states which dominate the photodynamics of adenine at shorter excitation wavelengths.[45] The destabilization of the $\pi\sigma^*$ state in bulk water was also postulated by Yamazaki and Kato, based

on MRMP2 calculations.[44] Therefore, we agree with the interpretation of Roberts and co-workers,[42] who stated that $\pi\sigma^*$ states might not be active in the photochemistry of adenine after excitation at wavelengths above 220 nm. Nevertheless, if the EDPT photorelaxation channel can be triggered in aqueous adenine by higher-energy pulses, we predict significant mechanistic similarities to the process described for microsolvated imidazole, AICN,[24] and AMOX.[25] This prediction is inferred from the PE surface calculations performed for the imidazole-$(H_2O)_5$ and adenine-$(H_2O)_5$ clusters and the mechanistic investigations conducted before.

Acknowledgments

This work was funded by the Grant 14-12010S from the Grant Agency of the Czech Republic and by the project CEITEC 2020 (LQ1601) with financial support from the Ministry of Education, Youth and Sports of the Czech Republic under the National Sustainability Programme II. Support from a statutory activity subsidy from the Polish Ministry of Science and Higher Education for the Faculty of Chemistry of Wrocław University of Technology is gratefully acknowledged. Part of the calculations was performed at the Wrocław Center for Networking and Supercomputing (WCSS) and Interdisciplinary Centre for Mathematical and Computational Modelling in Warsaw (ICM).

References

1 C. E. Crespo-Hernández, B. Cohen, P. M. Hare and B. Kohler, *Chem. Rev.*, 2004, **104**, 1977–2020.

2 K. Kleinermanns, D. Nachtigallová and M. S. de Vries, *Int. Rev. Phys. Chem.*, 2013, **32**, 308–342.

3 R. Improta, F. Santoro and L. Blancafort, *Chem. Rev.*, 2016, **116**, 3540–3593.

4 T. Gustavsson, R. Improta and D. Markovitsi, *J. Phys. Chem. Lett.*, 2010, **1**, 2025–2030.

5 A. L. Sobolewski and W. Domcke, *Europhys. News*, 2006, **37**, 20–23.

6 M. Barbatti, A. J. A. Aquino, J. J. Szymczak, D. Nachtigallová, P. Hobza and H. Lischka, *Proc. Natl. Acad. Sci.*, 2010, **107**, 21453–21458.

7 A. L. Sobolewski, W. Domcke and C. Hättig, *Proc. Natl. Acad. Sci.*, 2005, **102**, 17903–17906.

8 D. Shemesh, A. L. Sobolewski and W. Domcke, *J. Am. Chem. Soc.*, 2009, **131**, 1374–1375.

9 M. Dargiewicz, M. Biczysko, R. Improta and V. Barone, *Phys. Chem. Chem. Phys.*, 2012, **14**, 8981–8989.

10 A. L. Sobolewski, W. Domcke, C. Dedonder-Lardeux and C. Jouvet, *Phys. Chem. Chem. Phys.*, 2002, **4**, 1093–1100.

11 M. W. Powner, B. Gerland and J. D. Sutherland, *Nature*, 2009, **459**, 239–242.

12 S. Lobsiger, S. Blaser, R. K. Sinha, H.-M. Frey and S. Leutwyler, *Nature Chem.*, 2014, **6**, 989–993.

13 M. Barbatti and H. Lischka, *Phys. Chem. Chem. Phys.*, 2015, **17**, 15452–15459.

14 D. Tuna, A. L. Sobolewski and W. Domcke, *J. Phys. Chem. A*, 2014, **118**, 122–127.

15 R. Szabla, J. Campos, J. E. Šponer, J. Šponer, R. W. Góra and J. D. Sutherland, *Chem. Sci.*, 2015, **6**, 2035–2043.

16 D. Tuna and W. Domcke, *Phys. Chem. Chem. Phys.*, 2015, **18**, 947–955.

17 V. A. Spata, W. Lee and S. Matsika, *J. Phys. Chem. Lett.*, 2016, **7**, 976–984.

18 C. E. Crespo-Hernández, B. Cohen and B. Kohler, *Nature*, 2005, **436**, 1141–1144.

19 F. Plasser and H. Lischka, *Photochem. Photobiol. Sci.*, 2013, **12**, 1440–1452.

20 D. B. Bucher, C. L. Kufner, A. Schlueter, T. Carell and W. Zinth, *J. Am. Chem. Soc.*, 2016, **138**, 186–190.

21 M. Barbatti, *J. Am. Chem. Soc.*, 2014, **136**, 10246–10249.

22 S. Chaiwongwattana, M. Sapunar, A. Ponzi, P. Decleva and N. Došlić, *J. Phys. Chem. A*, 2015, **119**, 10637–10644.

23 X. Wu, T. N. V. Karsili and W. Domcke, *ChemPhysChem*, 2016, **17**, 1298–1304.

24 R. Szabla, J. E. Šponer, J. Šponer, A. L. Sobolewski and R. W. Góra, *Phys. Chem. Chem. Phys.*, 2014, **16**, 17617–17626.

25 R. Szabla, J. Šponer and R. W. Góra, *J. Phys. Chem. Lett.*, 2015, **6**, 1467–1471.

26 G. M. Roberts and V. G. Stavros, *Chem. Sci.*, 2014, **5**, 1698–1722.

27 M. N. R. Ashfold, B. Cronin, A. L. Devine, R. N. Dixon and M. G. D. Nix, *Science*, 2006, **312**, 1637–1640.

28 M. N. R. Ashfold, G. A. King, D. Murdock, M. G. D. Nix, T. A. A. Oliver and A. G. Sage, *Phys. Chem. Chem. Phys.*, 2010, **12**, 1218–1238.

29 A. L. Sobolewski and W. Domcke, *J. Phys. Chem. A*, 2001, **105**, 9275–9283.

30 A. L. Sobolewski and W. Domcke, *Chem. Phys. Lett.*, 2000, **321**, 479–484.

31 A. L. Sobolewski and W. Domcke, *Chem. Phys. Lett.*, 2000, **329**, 130–137.

32 W. Domcke and A. L. Sobolewski, *Science*, 2003, **302**, 1693–1694.

33 T. A. A. Oliver, Y. Zhang, A. Roy, M. N. R. Ashfold and S. E. Bradforth, *J. Phys. Chem. Lett.*, 2015,

6, 4159–4164.

34 M. Ataelahi, R. Omidyan and G. Azimi, *Photochem. Photobiol. Sci.*, 2015, **14**, 457–464.

35 R. Omidyan, Z. Heidari, M. Salehi and G. Azimi, *J. Phys. Chem. A*, 2015, **119**, 6650–6660.

36 M. Miyazaki, R. Ohara, K. Daigoku, K. Hashimoto, J. R. Woodward, C. Dedonder, C. Jouvet and M. Fujii, *Angew. Chem. Int. Ed.*, 2015, **54**, 15089–15093.

37 S. Hammes-Schiffer, *Energy Environ. Sci.*, 2012, **5**, 7696–7703.

38 T. Pancur, N. K. Schwalb, F. Renth and F. Temps, *Chem. Phys.*, 2005, **313**, 199–212.

39 F. Buchner, H.-H. Ritze, J. Lahl and A. Lübcke, *Phys. Chem. Chem. Phys.*, 2013, **15**, 11402–11408.

40 H.-H. Ritze, H. Lippert, E. Samoylova, V. R. Smith, I. V. Hertel, W. Radloff and T. Schultz, *J. Chem. Phys.*, 2005, **122**, 224320.

41 B. Cohen, P. M. Hare and B. Kohler, *J. Am. Chem. Soc.*, 2003, **125**, 13594–13601.

42 G. M. Roberts, H. J. B. Marroux, M. P. Grubb, M. N. R. Ashfold and A. J. Orr-Ewing, *J. Phys. Chem. A*, 2014, **118**, 11211–11225.

43 V. Ludwig, Z. M. da Costa, M. S. do Amaral, A. C. Borin, S. Canuto and L. Serrano-Andrés, *Chem. Phys. Lett.*, 2010, **492**, 164–169.

44 S. Yamazaki and S. Kato, *J. Am. Chem. Soc.*, 2007, **129**, 2901–2909.

45 F. Plasser, R. Crespo-Otero, M. Pederzoli, J. Pittner, H. Lischka and M. Barbatti, *J. Chem. Theor. Comput.*, 2014, **10**, 1395–1405.

46 S. Perun, A. L. Sobolewski and W. Domcke, *Chem. Phys.*, 2005, **313**, 107–112.

47 S. Perun, A. L. Sobolewski and W. Domcke, *J. Am. Chem. Soc.*, 2005, **127**, 6257–6265.

48 M. G. D. Nix, A. L. Devine, B. Cronin and M. N. R. Ashfold, *J. Chem. Phys.*, 2007, **126**, 124312.

49 M. Barbatti, Z. Lan, R. Crespo-Otero, J. Szymczak, H. Lischka and W. Thiel, *J. Chem. Phys.*, 2012, **137**, 22A503.

50 F. Weigend and R. Ahlrichs, *Phys. Chem. Chem. Phys.*, 2005, **7**, 3297–3305.

51 A. D. Becke, *J. Chem. Phys.*, 1993, **98**, 5648–5652.

52 B. Santra, A. Michaelides and M. Scheffler, *J. Chem. Phys.*, 2007, **127**, 184104.

53 B. Santra, A. Michaelides, M. Fuchs, A. Tkatchenko, C. Filippi and M. Scheffler, *J. Chem. Phys.*, 2008, **129**, 194111.

54 A. B. Trofimov and J. Schirmer, *J. Phys. B: At. Mol. Opt. Phys.*, 1995, **28**, 2299.

55 C. Hättig, *Advances in Quantum Chemistry*, Academic Press, 2005, vol. 50, pp. 37–60.

56 A. Dreuw and M. Wormit, *Wiley Interdiscip. Rev. Comput. Mol. Sci.*, 2015, **5**, 82–95.

57 T. H. Dunning, *J. Chem. Phys.*, 1989, **90**, 1007–1023.

58 R. A. Kendall, T. H. Dunning and R. J. Harrison, *J. Chem. Phys.*, 1992, **96**, 6796–6806.

59 B. G. Levine, J. D. Coe and T. J. Martínez, *J. Phys. Chem. B*, 2008, **112**, 405–413.

60 D. Tuna, D. Lefrancois, Ł. Wolański, S. Gozem, I. Schapiro, T. Andruniów, A. Dreuw and M. Olivucci, *J. Chem. Theory Comput.*, 2015, **11**, 5758–5781.

61 R. Crespo-Otero and M. Barbatti, *Theor. Chem. Acc.*, 2012, **131**, 1–14.

62 R. Crespo-Otero, M. Barbatti, H. Yu, N. L. Evans and S. Ullrich, *ChemPhysChem*, 2011, **12**, 3365–3375.

63 G. Granucci and M. Persico, *J. Chem. Phys.*, 2007, **126**, 134114.

64 R. Ahlrichs, M. Bär, M. Häser, H. Horn and C. Kölmel, *Chem. Phys. Lett.*, 1989, **162**, 165–169.

65 M. Barbatti, M. Ruckenbauer, F. Plasser, J. Pittner, G. Granucci, M. Persico and H. Lischka, *Wiley Interdiscip. Rev.: Comput. Mol. Sci.*, 2014, **4**, 26–33.

66 F. Calvo, M.-C. Bacchus-Montabonel and C. Clavaguéra, *J. Phys. Chem. A*, 2016, **120**, 2380–2389.

67 L. Serrano-Andrés, M. P. Fülscher, B. O. Roos and M. Merchán, *J. Phys. Chem.*, 1996, **100**, 6484–6491.

68 M. K. Shukla and J. Leszczynski, *J. Biomol. Struct. Dyn.*, 2007, **25**, 93–118.